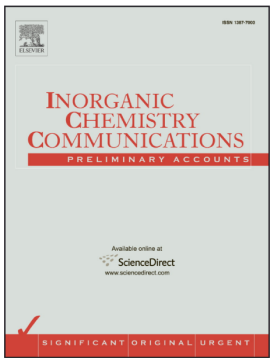

Household chemicals as key ingredients: the addition of sodium percarbonate to tin chloride in deep eutectic solvents leads to SnO2 nanoparticles very efficient for dye photocatalytic degradation

Lorenzo Gontrani, Francesca A. Cotirlan, Angelo Lembo, Elvira M. Bauer, Marilena Carbone

PII: S1387-7003(26)00213-3

DOI: https://doi.org/10.1016/j.inoche.2026.116347

Reference: INOCHE 116347

To appear in: *Inorganic Chemistry Communications*

Received date: 25 November 2025

Revised date: 30 January 2026

Accepted date: 12 February 2026

Please cite this article as: L. Gontrani, F.A. Cotirlan, A. Lembo, et al., Household chemicals as key ingredients: the addition of sodium percarbonate to tin chloride in deep eutectic solvents leads to SnO2 nanoparticles very efficient for dye photocatalytic degradation, *Inorganic Chemistry Communications* (2024), https://doi.org/10.1016/j.inoche.2026.116347

Household chemicals as key ingredients: the addition of sodium percarbonate to tin chloride in Deep Eutectic Solvents leads to SnO_2 nanoparticles very efficient for dye photocatalytic degradation

Lorenzo Gontrani*[,a], Francesca A. Cotirlan[a], Angelo Lembo[a], Elvira M. Bauer[b], Marilena Carbone[a]

a. STARTNETICS- Department of Chemical Science and Technologies, University of Rome Tor Vergata, Via della Ricerca Scientifica 1, 00133 Rome, Italy

b. Institute of Structure of Matter-Italian National Research Council (ISM-CNR), c/o Area della Ricerca di Roma1, Strada Provinciale 35d n. 9, Montelibretti, 00010 Rome, Italy.

Abstract

The combination of Deep Eutectic Solvents and inorganic synthesis has one of its highest expressions in the preparation of functional materials endowed with remarkable features and ensuing technological properties. In this contribution, we present a new simple and low-cost synthetic approach to synthesize tin dioxide nanoparticles in deep eutectic solvent reline that improves the method reported in the literature, which leads to tin monoxide. The new strategy is based on the addition of a readily available and low-cost oxidizing additive found in household materials (sodium percarbonate), and leads exclusively to high-purity dioxide. The two samples prepared (dioxide and control monoxide) were fully characterized with structural, spectroscopic and microscopy techniques. Both systems were found to contain bidimensional nanostructures, namely larger platelets aggregated in ice-cream scoops-like domains in SnO, and smaller low nm-range lozenges pillared on top of each other in SnO_2. Both oxides were tested as photocatalysts in the degradation of crystal violet dye in various conditions, obtaining exceptional results for tin dioxide in terms of degradation times, remarkably shorter than literature values.

1. Introduction

Water pollution caused by synthetic dyes poses a significant environmental challenge, as these compounds are often highly stable, toxic and non-biodegradable, and very often their disposal is inappropriate. Among the most common pollutants, Crystal Violet dye (CV) plays a significant role, considering its widespread use and easy availability. This triphenylmethane dye has a variety of uses, such as in the textile processing industry, as a biological stain, and to give paintings and printing ink a rich violet hue. CV is known for the large number of adverse effects it can exert on humans, as well as on other living beings and on the environment [1], ranging from its mutagenic to mitotic toxicity, [2–4] that make it a serious biohazard; it was also described as potentially carcinogenic [5,6]. The molecule imparts various eye-related problems like irritation [7], conjunctiva and cornea injury [8,9]. On prolonged exposure, it can cause respiratory ailment, kidney failure, permanent blindness and cancer [10]. Therefore, pollution from CV poses a serious problem to countries where textile industries are a major asset of the economy [11,12] and its removal from wastewater is highly desirable. The development of a methodology for removing CVs from polluted water that can be implemented very quickly, is easy to manage with minimal equipment, has a negligible environmental impact (should not cause further environmental contamination), and is very inexpensive is of paramount importance, especially considering that most of the textile industries in which the dye is widely used are often located in countries with limited economic resources. Several methods for dye removal have been proposed, including bioremediation using bacteria strains [13], electrocoagulation by generating adsorbing Fe and Al hydroxides *in situ* [14], direct chemical degradation through Fenton-like methodologies [15], photocatalysis [16] and adsorption [17–20]; the latter two methods will be exploited in the present study. Among the compounds employed for this purpose, metal oxides are often chosen, in particular for water and air purification [21], due to their ability to oxidize contaminants. Nanoparticles perform better than bulk materials owing to their greater reactive surface area [22,23], which is anticorrelated to the particle size, and directly affects the ability to adsorb and remove pollutants [16].

In this study, tin monoxide (SnO) and dioxide (SnO_2) were synthesized in nanoparticle form by precipitation reactions using choline chloride-urea 1:2 Deep Eutectic Solvent (DES) as reaction medium, and the two materials' efficiency in removing CV from its water solutions was evaluated. These two systems were chosen among all available tin oxides SnOx as "simple" prototypes; as a matter of fact, tin gives origin to a large number of composition when reacting with oxygen, either with intermediate oxidation states, [24,25], like Sn_2O_3 [26], Sn_3O_4 [27] and Sn_5O_6 [28], or non-stoichiometric [29]. SnO and SnO_2 are the only two oxides naturally found in minerals. The former is rarer than the latter, and is found in the minerals romarchite/hydroromarchite [30] whereas the latter is remarkably more common and constitutes the mineral cassiterite [31], historically the main source of tin. More specifically, tin monoxide has a dark color (tending to black), is slightly paramagnetic and insoluble in water, has a tetragonal unit cell with a stratified structure, also called lithargic [32], where each tin atom is coordinated with four oxygen atoms and contains asymmetrical sites with four Sn coordinates. [33] This material is a p-type semiconductor endowed of a 2.7 eV electronic band gap, and finds several uses electronic devices, such as gas sensors and catalysts [34]. Tin dioxide is, on the contrary, an n-type semiconductor, with a band gap of about 3.6 eV [35]; such features are at the basis of the many technological devices where the material is involved, like transparent conductive systems [36,37], catalysts [38,39] and solid-state gas sensors [40,41]. SnO_2 is light in color (it is normally described as "off-white"), is insoluble in water and is odorless. In the solid state it contains a tetragonal unit cell with the structure of rutile [42] where tin is hexa-coordinated to oxide anions. Such structure promotes the adsorption of molecules and ions, since channels and adsorption sites are formed on the surface of the crystal, allowing for capturing and retaining of the adsorbates [43,44].

The analysis of the materials catalytic activity was conducted considering both adsorption and photocatalysis, under different operative conditions: dark, ambient light, visible and UV light. Such dual experiment was carried out since both synthesized materials show a certain adsorptive capacity, leading to a decrease in dye concentration even in the absence of light; yet, the effect of light shining was always remarkable, with SnO_2 showing a greater removal capacity than SnO in all four experimental conditions employed. The results obtained also show a considerable influence on the type of lighting, and reach particularly significant removal values when UV light is used in conjunction with SnO_2, in line with the electronic properties of the latter. This study suggests that the combined use of adsorption and photocatalysis could represent an effective and synergistic strategy for the removal of pollutant dyes and paves the way for possible applications in wastewater treatment.

Particularly valuable for the sustainability of the entire water remediation cycle is the low-impact "wet" synthesis used to prepare the materials, which involved the use of low-toxicity, low-temperature environment (DES). This route avoids the use of high temperature "dry" methods, as it happens, e. g., when the oxide is the final product of high-temperature thermal treatments, like hydrothermal reactions followed by calcination [45,46]. The novelty of DESs lies in their microscopical structure, that is mainly based on the establishment of a large network of intermolecular interactions - mostly hydrogen bonds between donor (HBD) and acceptor (HBA) groups – which favors the formation of a liquid phase at mild temperatures and requires only little heating if any. Although macroscopically homogeneous, DESs feature the alternation of domains of different type at the nanoscopic level (charged, polar, neutral moieties, voids), which imparts remarkable heterogeneity to the system [47–51]. These characteristics can facilitate anisotropic crystal formation and guide nucleation paths, allowing templating effects without the use of exogenous surfactants or post-synthesis treatments [52,53]. These attractive features have fostered great interest in the inorganic materials community, and an increasing number on DES-assisted syntheses of nanomaterials has been reported in the literature in the last few years [54,55]. Concerning the preparation of metal oxides, several strategies have been proposed using the most common choline-based eutectic mixtures with chemical [56], and electrochemical syntheses [57–59] and Lewis acids-based DESs, like zinc nitrate:urea mixtures, where ZnO with platelet/sheet-like morphologies was achieved under mild conditions [52]

2. Materials and Methods

All chemicals used in the present work are commercially available and were used without further purification: Choline chloride (ChCl - $[(CH_3)_3NCH_2CH_2OH]^+Cl^-$, CAS n. 67-48-1, Alpha Aesar), Urea CAS n. 57-13-6, Fluka, Dihydrated tin dichloride ($SnCl_2 \cdot 2H_2O$, CAS n. 10025-69-1, Merck), Sodium percarbonate (SPC - $2Na_2CO_3 \cdot 3H_2O_2$, CAS n. 15630-89-4, Riedel-de Haën); Crystal Violet (C_{25} H_{30} Cl N_3, CAS n. 548-62-9, Tokyo Chemical Industry (TCI)). p-BQ (parabenzoquinone) CAS n. 106-51-4, Merck-Sigma Aldrich. All the chemicals were at analytical grade (>95% purity); doubly distilled water (dd-H_2O) was used throughout the washing procedures.

For the synthesis of the two tin oxides, the method proposed by Zheng and colleagues [60]was taken as starting point: for SnO the protocol was followed as reported, while for SnO_2 sodium percarbonate (SPC), was added in order to create a highly oxidizing environment, with the aim of obtaining the metal in its highest oxidation state (+4). This general synthesis protocol exploits the capabilities of Deep Eutectic Solvents (DES) of acting as solvent, reactant and templating agent at the same time [61]. For a general discussion on the properties of these innovative solvent media, the reader is referred to the large number of articles/reviews published in the last decade. [62–70]

2.1 SnO Synthesis

The liquid DES system used for the synthesis as active reaction medium, was prepared by mixing ChCl and urea at a 1:2 stoichiometric ratio, shaking and heating at about 40°C until a colorless homogeneous liquid was formed. In a screw-capped vial containing 2.5 mL of this DES, 0.154 g of $SnCl_2 \bullet 2H_2O$ were added at room temperature; the system was then heated in oil bath at 100°C. After a short time (less than 5 min), a brown colloid started to form and precipitate. To be sure of the completeness of the reaction, the reaction time was set at two hours; the precipitate was collected afterwards adding small quantities of deionized water. The dark grey solid was washed and centrifuged with distilled water to remove the excess of unreacted DES until the pH value of the supernatant

2.2 SnO_2 synthesis

The same DES (ChCl/urea in 1:2 molar ratio) used to prepare SnO was employed, and added with $SnCl_2 \bullet \cdot 2H_2O$ as described above. Once the oil bath reached 100°C, SPC was added to the DES solution, according to 1:3 Sn:SPC stoichiometric ratio. Sodium percarbonate is a powerful oxidizing mixture, consisting in a 2:3 adduct between Na_2CO_3 and hydrogen peroxide (H_2O_2), that finds widespread use as household chemical under different brands. This can be considered as a strong but relatively green and harmless oxidant, since the reaction products are water and molecular oxygen. SPC use within tin dioxide synthesis was devised in order to create and maintain a strongly oxidizing environment that could boost the conversion of the tin compound formed towards the highest oxidation state. The choice of the 1:3 Sn:SPC ratio resulted from a trial-and-error investigation, that assessed that pure SnO_2 cannot be formed at lower ratios, as it was verified using the two compositions 1:1 and 1:2, that led to SnO, with SnO_2 present only in traces. The reaction mixture was placed in the oil bath, brought to 100°C and at that temperature the precipitation reaction begins, which is conducted for a total of two hours. During this time, the reaction mixture varies in color from an off-white to a creamy white, tending to a light yellow. At the end of the reaction, the precipitate was treated with water through a series of washings/centrifugation until the pH value of the supernatant was reduced at around 7. Once the washing was finished, the precipitate was left to dry at room temperature, yielding an off-white solid. Plausible mechanisms for SnO and SnO_2 synthesis under these experimental conditions could include a series of steps. Tin chloride at neutral/basic pH can form tin oxychloride by reacting with the precursor crystal water and environmental humidity, and can then be converted into SnO by reaction with the (tiny) quantity of ammonia originated from urea partial decomposition (scheme 1): [60],

$$SnCl_2 + H_2O \rightarrow Sn(OH)Cl + HCl$$

$$CO(NH_2)_2 \rightarrow NH_3 + HCNO \quad (1)$$

$Sn(OH)Cl + NH_3 \rightarrow 2SnO + 2NH_4Cl$

It is believed that, in tin dioxide preparation, these first three steps, common to both syntheses are ensued by the reaction of SnO with either molecular oxygen formed *in situ* by SPC/H_2O_2 decomposition (a), or directly with the peroxide, that can oxidize tin (II) in the basic environment granted by carbonate anion (b), as it was verified by qualitative pH measurements (scheme 2):

$2Na_2CO_3 \cdot 3H_2O_2 \rightarrow 3H_2O_2 + 4Na^+ + 2CO_3^{2-}$

(a) $2H_2O_2 \rightarrow 2H_2O + O_2$

$2SnO + O_2 \rightarrow 2SnO_2$ (2)

(b) $Sn^{2+} + H_2O_2 + 2OH^- \rightarrow 2SnO_2 + 2H_2O$

2.3 CV solution

To prepare the aqueous solution of CV, 0.9 mg of powdered CV were weighed, and then dissolved in 100 mL of deionized water in a flask, so as to obtain a final concentration of 9 ppm ($2.197 \cdot 10^{-5}$ mol/litre). In order to slow down the degradation due to light, the solution was stored in a brown glass container.

2.4 Instrumentation

The synthesized powders were analysed in a Field Emission Microscope Zeiss Auriga 405, 1 nm nominal resolution (Oberkochen, Germany), mounting a Gemini column and operating at 7 kV and equipped with a Bruker Quantax energy dispersive X-ray spectroscope (Energy Resolution: 123 eV at Mn Kα line). The observation was performed under high vacuum ($10^{-5} \div 10^{-6}$ mbar). The microanalysis was carried out at accelerating voltage E_0 =3, 5, 10, 15 keV. Images were recorded on both fine powder samples precipitated from a drop of water dispersions of the sample (drop-cast method) and on small portions of the solid powder with no further treatment. Aluminium stubs were used as sample holders in both cases. Powder-XRD patterns were collected in transmission geometry with an X'pert pro X-ray diffractometer by Philips, using Cu Kα (l = 1.5407 Å) radiation. Primary data were processed performing the necessary corrections for the background and sample absorption, and the scattered intensity was obtained in the 10-90 2θ angular range. Infrared spectra were recorded with a Shimadzu Prestige-21 FT-IR instrument, equipped with an attenuated total reflectance (ATR) diamond crystal (Specac Golden Gate), in the range 400-4000 cm^{-1}, with a resolution of 4 cm^{-1}. Ultraviolet-visible (UV-Vis) spectra were recorded on a Varian Cary 50 Scan spectrophotometer, equipped with Cary Win UV Scan software. The irradiance of the in-house assembled white lamp used in the kinetics experiment was measured with an optical bench instrumentation, and resulted to be 89 mW a 590 nm (CV absorption maximum); the professional UV torch employed features a 4-core 365 nm UV LED source (power 30 W), equipped with a multi-layer filter optical lens that filters ambient light up to 99% to make UV light purer.

2.5 UV-Vis experiments design

The analysis on dye removal from the aqueous solution with CV employing the two synthesized tin oxides was performed under four different experimental conditions: 1) dark 2) ambient illumination (neon bulb), white lamp and UV lamp (see Materials and Methods for details). For each experiment, 3 mg of tin monoxide or tin dioxide and 3 mL of water containing CV were used, in order to have 1 mg/mL concentration in every sample, useful for making comparisons among the different cases. The mixture was placed inside a beaker and was left under magnetic bead stirring for multiples of fixed amounts of time (3 minutes) under illumination or not. At the end of each time slot, the solution was centrifuged and the UV-Vis spectrum of the supernatant was registered. Centrifugation was necessary in order not to have scattering signals in the spectra, caused by the dispersion of the two oxides in solution. Overall,

the total time of the measurements, starting from the initial time (t0) before any stirring, up to last point t21 was 21 minutes, for a total of 8 points sampled per experiment.

In the mechanistic study (superoxide radical assessment), a 30 μM solution of *p*-BQ (parabenzoquinone) in ACN (acetonitrile) or water (3 mL total volume) was added with 3.0 mg of SnO_2 and mixed for few seconds (15-20), then the suspension was centrifuged at 14500 rpm for 1 minute, and the supernatant was used to record the UV-Vis spectrum corresponding to the starting point (time point 0 min). Afterwards, the supernatant and the centrifuged nanoparticles were joint together and the obtained suspension was sonicated for 15 seconds before the measurement. During irradiation the suspension was left under vigorous stirring (750 rpm) in oxic conditions (in air).

3. Results and discussion

3.1 Fourier transform infrared spectroscopy (ATR-FTIR)

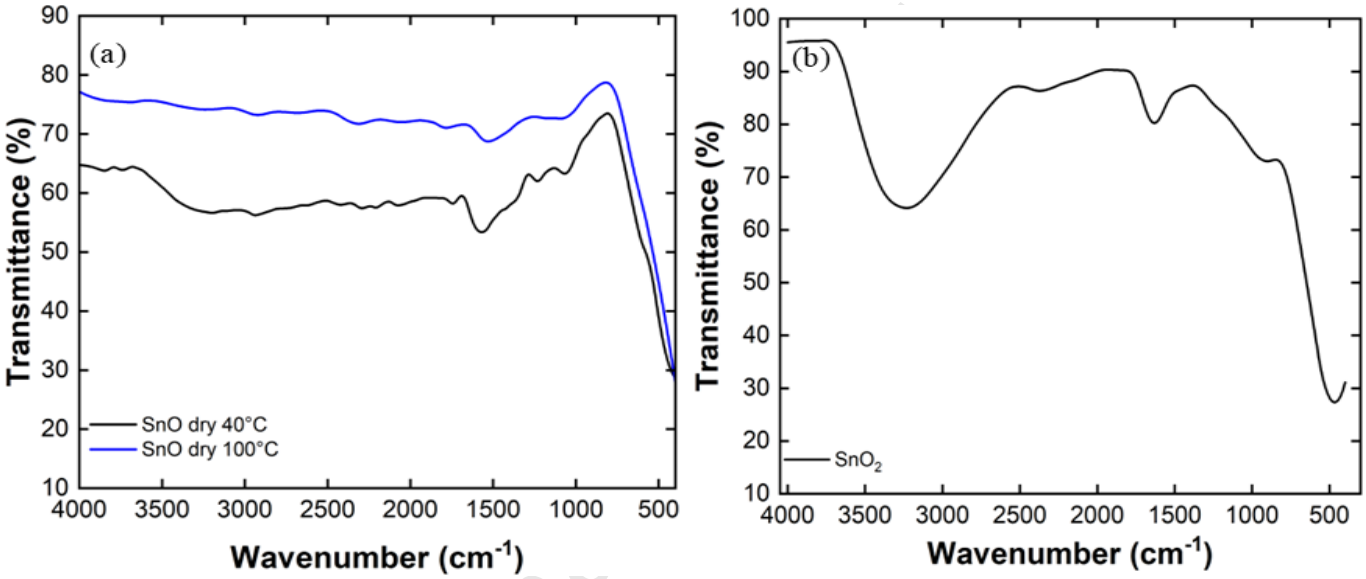

Figure 1 IR-ATR spectrum of SnO (a) and SnO_2 (b) samples

IR spectroscopy analysis was performed to identify and characterize the chemical compounds under investigation. The IR spectra of the synthesized samples were obtained in the wavenumber range 4000-400 cm^{-1}. In this wavenumber range, SnO and SnO_2 have different absorption spectra due to their different chemical structures and consequent molecular vibrations. The most prominent feature observed in infrared spectra of both the synthesized tin oxides (Fig 1, SnO panel a, SnO_2 panel b), is the characteristic absorption observed in the rightmost part of the pattern, that is originated by the stretching normal mode of Sn-O bond; this feature is observed at around 410 cm^{-1} in SnO and around 480 cm^{-1} in SnO_2. This small but sizeable shift is one of the fingerprints used to distinguish between the two compounds, together with the different XRD pattern. In the ATR-FTIR spectrum recorded for SnO dried at 40°C, other noteworthy features appear, namely the O-H stretching (between 3000 and 3500 cm^{-1}) and bending (around 1600 cm^{-1}) bands related to the presence of adsorbed water [71]. Such absorptions are strongly reduced when SnO is treated at 120°C for about two hours, suggesting that they were originated by superficial water and not to more tightly held crystal water. In the IR spectrum of SnO_2 sample, besides the already cited Sn-O stretching peak now at 480 cm^{-1}, more intense and better defined absorption signals are found at 3250 and 1600 cm^{-1}. This feature may suggest a more ordered adsorbed water layer, brought about by the higher adsorption capacity of dioxide compared to the monoxide, as it can be appreciated in the following paragraphs.

3.2 X-Ray diffraction (XRD)

The synthesized samples of synthesized monoxide and tin dioxide were analysed by XRD in order to identify the structure of the molecules contained and to confirm their identity.

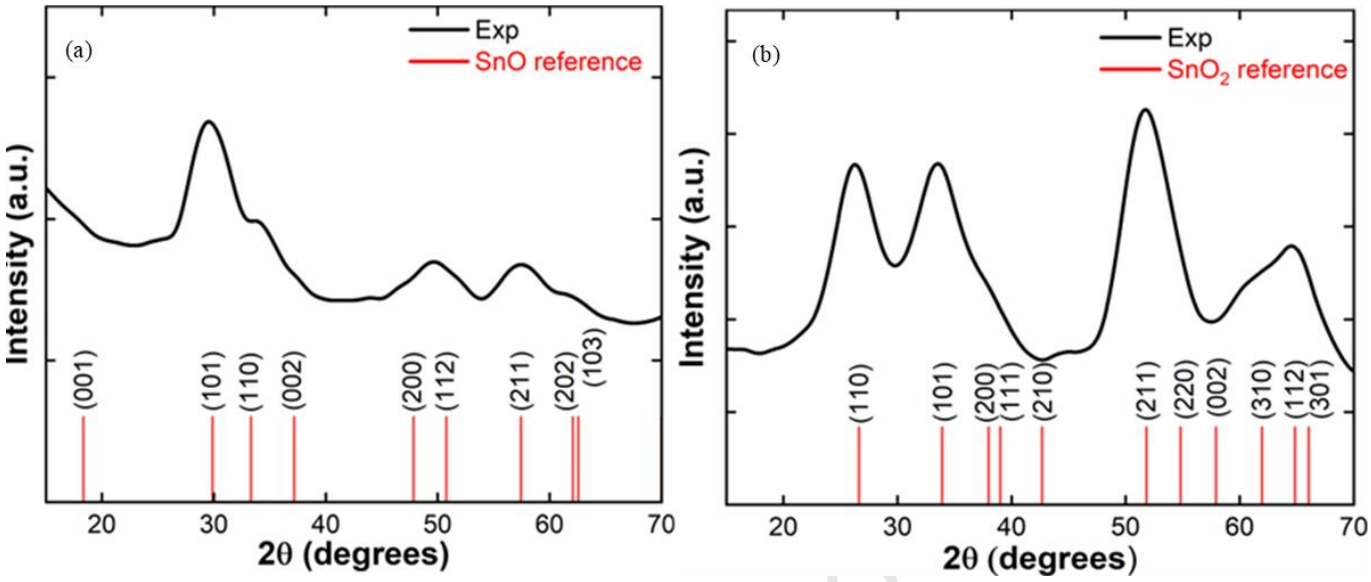

Figure 2 Diffractogram of SnO (a) and SnO_2 (b) samples

In all graphs (Fig. 2), the experimental pattern is shown in the 2θ range of between 10 and 70°, and the positions of the peaks (reflections) of the reference crystal structures of SnO and SnO_2, taken from the American Mineralogist database, are plotted as red vertical lines. In SnO spectrum (left panel), four evident wide peaks appear at 2θ = 29.88°, 33.32°, 50.76° and 57.43°. Notwithstanding the peak's width, it is actually possible to find a strong correspondence with the reflections found in the reference mineral romarchite, corresponding to lattice planes 101, 110, 112 and 211, also taking into account the dimension of the nanocrystallites (nanoparticles), that lead to peak broadening. Turning to SnO_2 XRD spectrum (Fig 2, panel b), the most intense peaks are seen at 2θ= 26.61°, 33.92°, 51.83° and 64.83°. Again, it is possible to observe a very good compliance with the reflections originated by diffraction from 110, 101, 211 and 112 crystal planes of the reference mineral cassiterite [31] (tetragonal lattice). In the end, it was found that both SnO and SnO_2 have a tetragonal crystal structure, in accordance with the literature. Yet, the two phases are well distinguished thanks to the positions of XRD peaks, in particular it can be seen that SnO has a single strong peak centered at 30°, while in SnO_2 the peak turns into a double peak (about 27° and 34°). This characteristic is distinctive and is consistent with what is reported in the reference databases (American Mineralogist, Crystallographic Database, FIZ Karlsruhe: SnO ICSD 424729 [72], SnO_2 ICSD 2398260 [73]). The comparison between the two mineral powder patterns is reported in the supplementary material – Fig. SI1.

3.3 Scanning Electron Microscopy (SEM)

SEM analysis was performed in order to assess the presence of nanoparticles, and to estimate/quantify their topology (i. e. shape and size). SEM analyses were performed both on powders and on water dispersion (concentration 1 mg/mL). In both experiments, carbon tape disks glued to aluminium stubs were used as sample holder, with either direct deposition on the adhesive (powder) or drop-casting (dispersion). Different magnifications, ranging from 4000 to 100000X, were operated.

Typical SEM images collected for SnO samples are shown in Fig. 3. At medium magnification (13kX, panel b), the material appears to contain hollow and reticulated spheres, aggregated in a spongy structure. At higher magnification (59 kX, panel b) a more complex internal structure is revealed, and the "ice-cream scoops" appear clearly to be made of nanometrical 2D platelets (about 2-300 nm (long edge) x 2-30 nm (short edge)), with a fairly large exposed surface. Regarding SnO_2, the collected SEM images (shown in Fig. 4 at 20 kX – panel a and 100 kX – panel b) show the

presence of pillars composed of small lozenge-shaped nanoplatelets lying on top of one another; the scabrousness of this morphology suggests a large surface area to the sample. The size distribution of these nano-objects (see supplementary information, Fig. SI2) is slightly positively skewed, with mean/modal values around 65 nm.

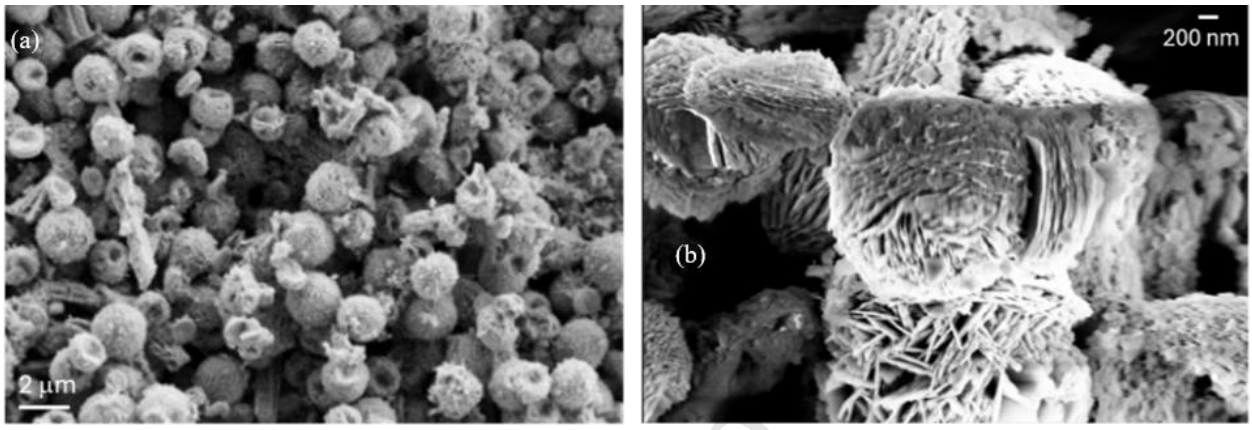

Figure 3: Selected SEM images of SnO powder at medium (a) and high magnification (b)

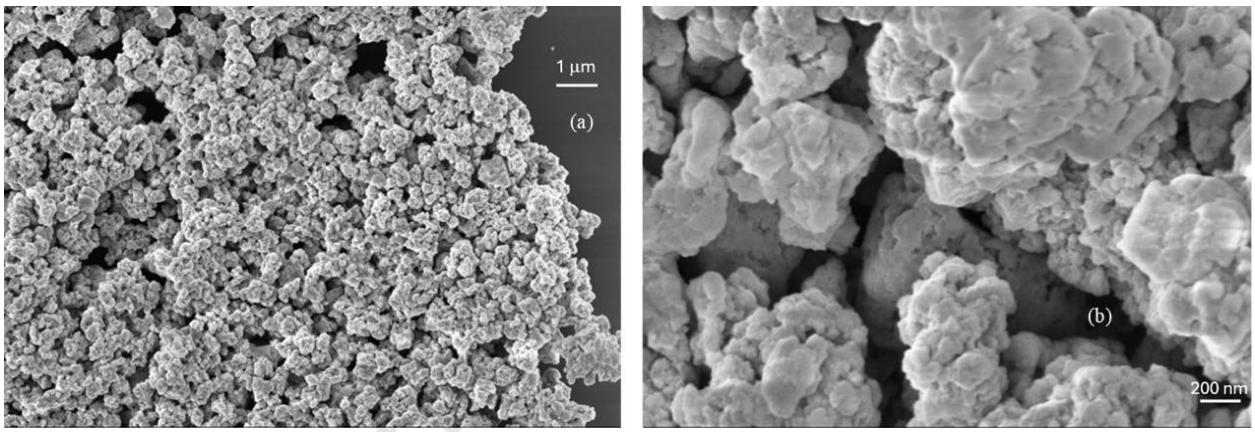

Figure 4 Selected SEM images of the SnO_2 sample at medium (a) and high magnification (b)

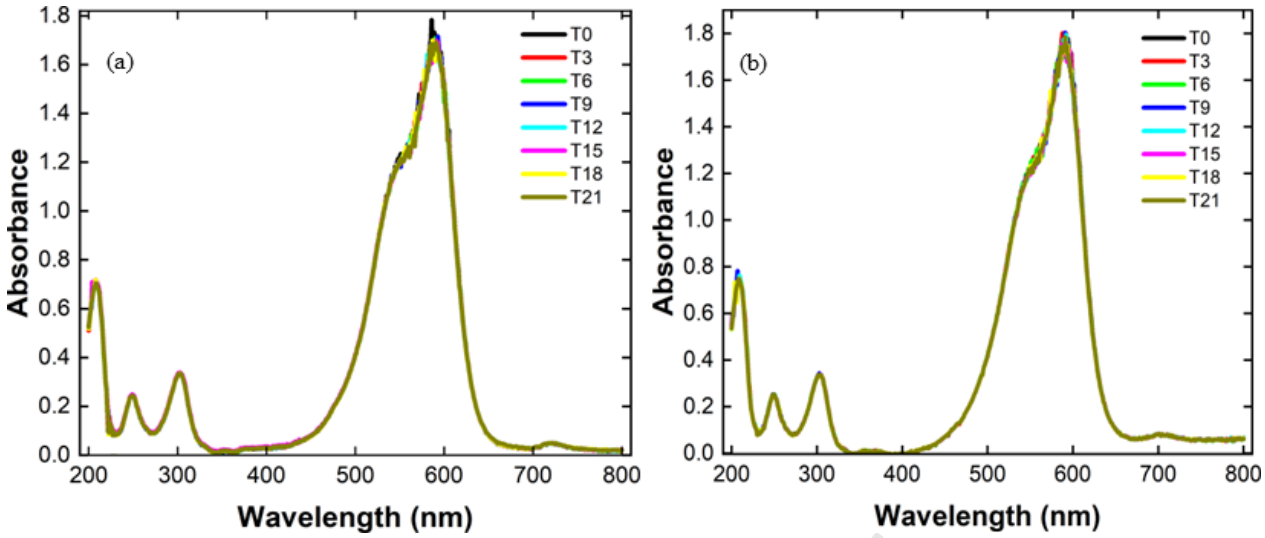

Figure 5 UV-Vis spectra of pure CV solution, showing the stability of the dye with no catalyst over time in dark (a) and under UV irradiation (b).

3.4 UV-visible spectroscopy

For the comparison between the experimental spectra recorded in the different operating conditions, the maximum absorption value of the CV, which falls at 590 nm, was considered, in order to maximize signal/noise ratio. The UV-visible spectra of CV solution with no added catalysts after different time lapses are all largely superimposable. In Fig. 5, the two extremal cases (dark and UV light) are shown, while the remaining spectra (ambient and white light) are reported in the supplementary material figure S3. Overall, the dye can be regarded as highly (photo)stable, as already discussed in the literature [74]; actually, the self-degradation under sun light in the absence of any catalyst, was found to be 1.9% at maximum in a very recent report [75]. Passing to the experiments in presence of the two tin oxide powders, the measurements performed with SnO are shown in Fig. 6, for all the four experimental conditions, and in Fig. 8, panel a. In the former picture, the entire absorbance spectra from 200 to 800 nm are overlapped, while in the latter the decrease of the maximum absorbance (at 590 nm) with increasing treatment time is reported for all the four experiments. It can be seen that in any of the four conditions some CV removal is observed, but only with ultraviolet light irradiation of a greater decrease in the absorbance value can be observed. The UV-visible spectra of the CV in the presence of the SnO_2 sample in the four experimental conditions are then reported in Fig. 7 and Fig. 8, panel b; also for this oxide, in the former case the total spectra are overlapped, whereas in the latter the time-dependent patterns are shown. Again, CV removal can be appreciated in all four conditions, with the most relevant and marked decolouring effect observed when UV light is shone. In addition, it can be noticed that the use of tin dioxide causes a much sharper decrease in the absorbance value than monoxide. In general, the introduction of tin oxide (SnO or SnO_2) into the system significantly modifies the CV removal process, both under irradiation and in the absence of light. In addition, the nature of the light source plays a primary role in the absorbance quenching. In particular, the use of ultraviolet radiation, regardless of the type of tin oxide used, promotes a more efficient removal of CV than visible light. To quantify the different capabilities of the two tin oxides in decreasing the pollutant concentration, it is convenient to define a metrics such as the removal percentage, which is defined as:

$$\%\text{removal} = \frac{C_0 - C}{C_0} \cdot 100 \qquad (3)$$

where C_0 is the initial absorbance and C is the final absorbance (at t21, i. e. after 21 minutes). The percentages of dye removal for each experiment are shown in the following table 1. The results reported above are indeed quite relevant,

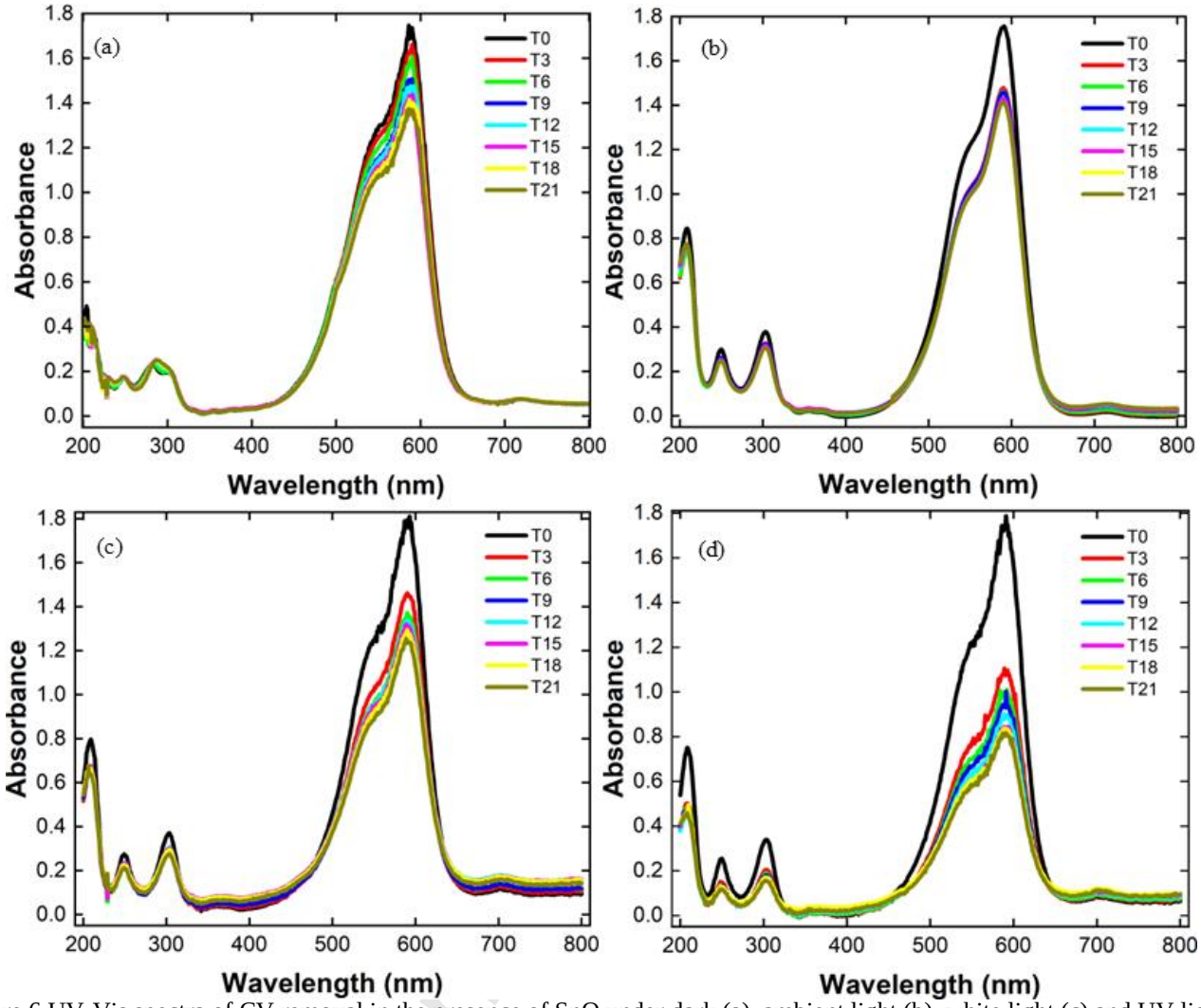

Figure 6 UV-Vis spectra of CV removal in the presence of SnO under dark (a), ambient light (b), white light (c) and UV light (d)

and show that SnO_2, in particular, is capable of removing almost completely the dye from the solution, totalling a champion 96% removal percentage after 21 minutes. These results can be compared to those reported by Shabna and coworkers [76], who used an SnO_2 sample synthesized with sol-gel methods as catalyst. In that work, the reported color removal was 47% in 75 minutes. Our very promising result can be attributed to the very large adsorption capabilities of the small-sized and highly porous nanostructure synthesized with our DES+SPC method, coupled to very efficient triggering of the light-induced radical-driven oxidation phenomena. The former phenomenon (adsorption) is detailed in table 2, that shows the absorbance quenching data recorded for CV+ catalyst solutions in dark. The percent absorbance reduction observed was correlated to the dye concentration change by applying the Lamber-Beer law with a molar extinction coefficient of 74277 L mol^{-1} cm^{-1}, which was obtained through a calibration curve employing various CV concentrations (see Fig. SI4 of the additional material). From the residual CV concentration, given the initial amount of catalyst (3 mg), the adsorption capability of the two oxides' powders (expressed as mg of dye per mg of oxide) could be obtained. The analysis shows that both compounds can adsorb CV in the observed time lapse; the effect is more marked in SnO_2, that can adsorb 0.17 mg of CV per mg of powder across the experiment duration (21 minutes); the difference between the two materials is likely related to the smaller dimensions of nanoparticles and to the ensuing larger surface in the dioxide. Concerning the experiment under illumination, the significant diversity of SnO and SnO_2 profiles suggest a pivotal role of the materials electronic

	No cat	CV+SnO	CV+SnO_2
Dark	2%	22%	42%
Neon bulb	3%	20%	76%
Visible light	2%	35%	89%
UV light	1%	59%	96%

Table 1: CV removal percentage values after 21 minutes of treatment

	CV+SnO		CV+SnO_2	
Time interval	%Abs decrease	Die/Cat adsorbed (mg/mg)	%Abs decrease	Dye/Cat adsorbed (mg/mg)
T3	4.55	0.01	7.38	0.02
T6	7.72	0.02	15.18	0.05
T9	13.89	0.04	23.51	0.07
T12	16.81	0.05	29.32	0.09
T15	18.09	0.05	34.06	0.10
T18	22.08	0.07	37.95	0.11
T21	22.14	0.07	41.96	0.13

Table 2: CV removal in dark, expressed as % absorbance decrease and adsorbed dye/catalyst mass ratio

structure (bandgap values). Following on from several studies [77], a cascade reaction featuring reactive oxygen species (ROS) like the following (scheme 4) can be hypothesized for the photodegradation mechanism [78,79]:

$$SnO_X + h\nu \rightarrow e^- + h^+$$
$$h^+ + H_2O \rightarrow \bullet OH + H^+$$
$$h^+ + OH^- \rightarrow \bullet OH$$
$$O_2 + e^- \rightarrow \bullet O_2^- \quad (4)$$
$$\bullet O_2^- + 2H^+ \rightarrow \bullet HO_2$$
$$\bullet O_2^- + e^- + 2H^+ \rightarrow H_2O_2$$
$$\bullet O_2^-/\bullet OH/H_2O_2 + CV \rightarrow \text{degradation products } (+ CO_2 + H_2O)$$

4. Photobleaching mechanism assessment

In order to understand which mechanism is responsible for CV dye bleaching, we focused our attention on SnO_2 and irradiation with UV-lamp at λ_{exc} = 365 nm. In principle, besides the two mechanisms reported in Scheme 4, also the formation of the singlet oxygen should be taken into account, however, this mainly occurs with organic dye sensitizers such as fluoresceine derivatives [80–82] and porphyrins [83–85], to name a few, while the generation of superoxide anion ($\bullet O_2^-$) still remains the most probable way to generate ROS with metals oxides [86,87]. In both cases it is possible to assess the formation of the different oxygen reactive species by indirect methods using diphenylisobenzofurane (DPBF) as singlet oxygen quencher [88–91], and *para*-benzoquinone (*p*-BQ) as radical scavenger [88,92,93] We focused our attention to this latter case and started the investigation with *p*-BQ in water, to switch then to a non protic solvent such as acetonitrile (ACN).

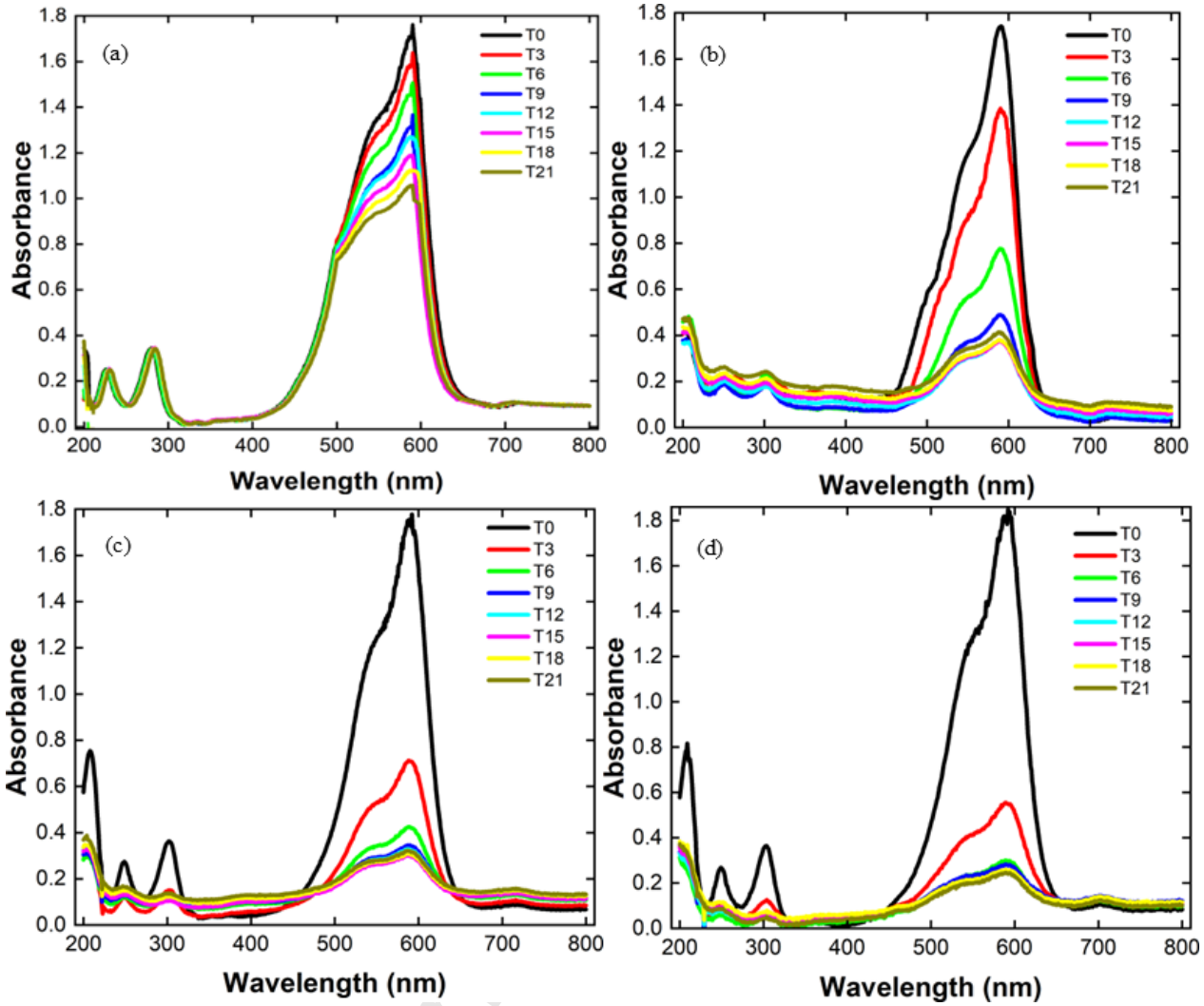

Figure 7 UV-vis spectra of CV removal in the presence of SnO_2 under dark (a), ambient light (b), white light (c) and UV light (d)

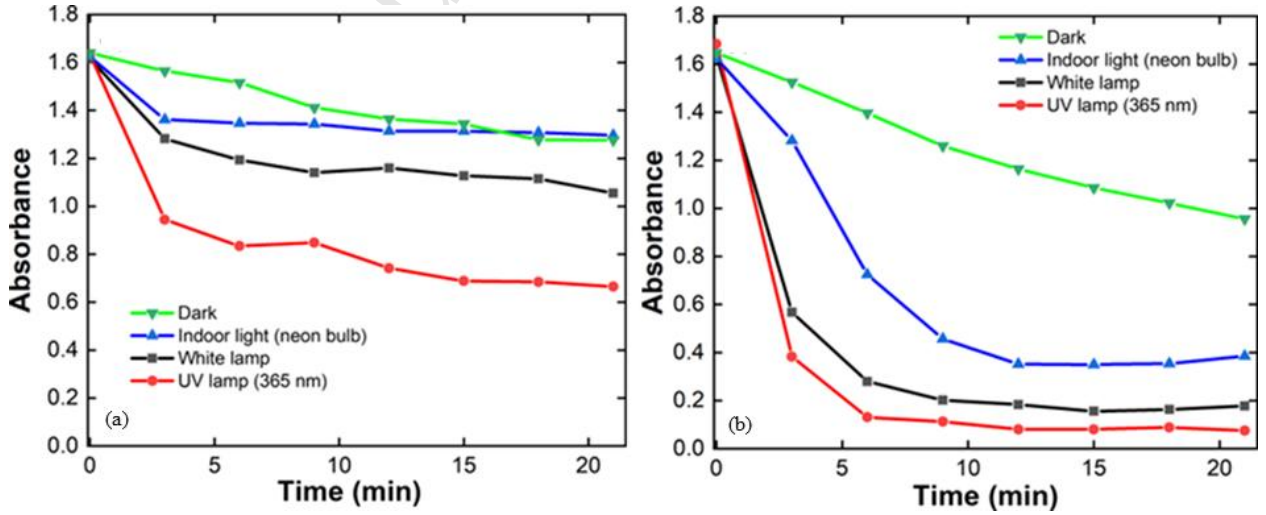

Figure 8 Plots of maximal absorbance values (at 590 nm) as a function of time in the presence of SnO (a) and SnO_2 (b) in the four experimental conditions.

As it is possible to see in Figure 9, panel a, the spectral changes of a non irradiated 30 µM solution of *p*-BQ in water with SnO_2 at 1mg/ml within 21 minutes, reveal partial physical adsorption of the molecule on the metal oxide surface, underlined by the decreasing absorbance value at 245 nm, despite the increasing absorbance below the 300 nm due to the SnO_2 nanoparticles, well suspended in solution thanks to the hydrogen bond interactions with water. When the solution is irradiated at 365 nm, with or without SnO_2 nanoparticles (Figure 9 panel b and c, respectively), very similar spectral features emerge. In both cases it is possible to discern the complete disappearance of the starting maximum peak at 245 nm, confirming the complete consumption of *p*-BQ, and, at the same time, new bands at 210, 260 and 490 nm arise. These spectral features are in good agreement with the presence in solution of 1,2,4-trihydroxybenzene (1,2,4-THB, absorption at 210 and 250-290 nm), 2-hydroxybenzoquinone (2-HO-BQ, absorption at 490 nm) and 2,5-dihydroxybenzoquinone (2,5-HO-BQ, absorption at 290 and 490 nm) as degradation products coming from the photolysis of *p*-BQ in water (Figure 9, panel d)[94–96].

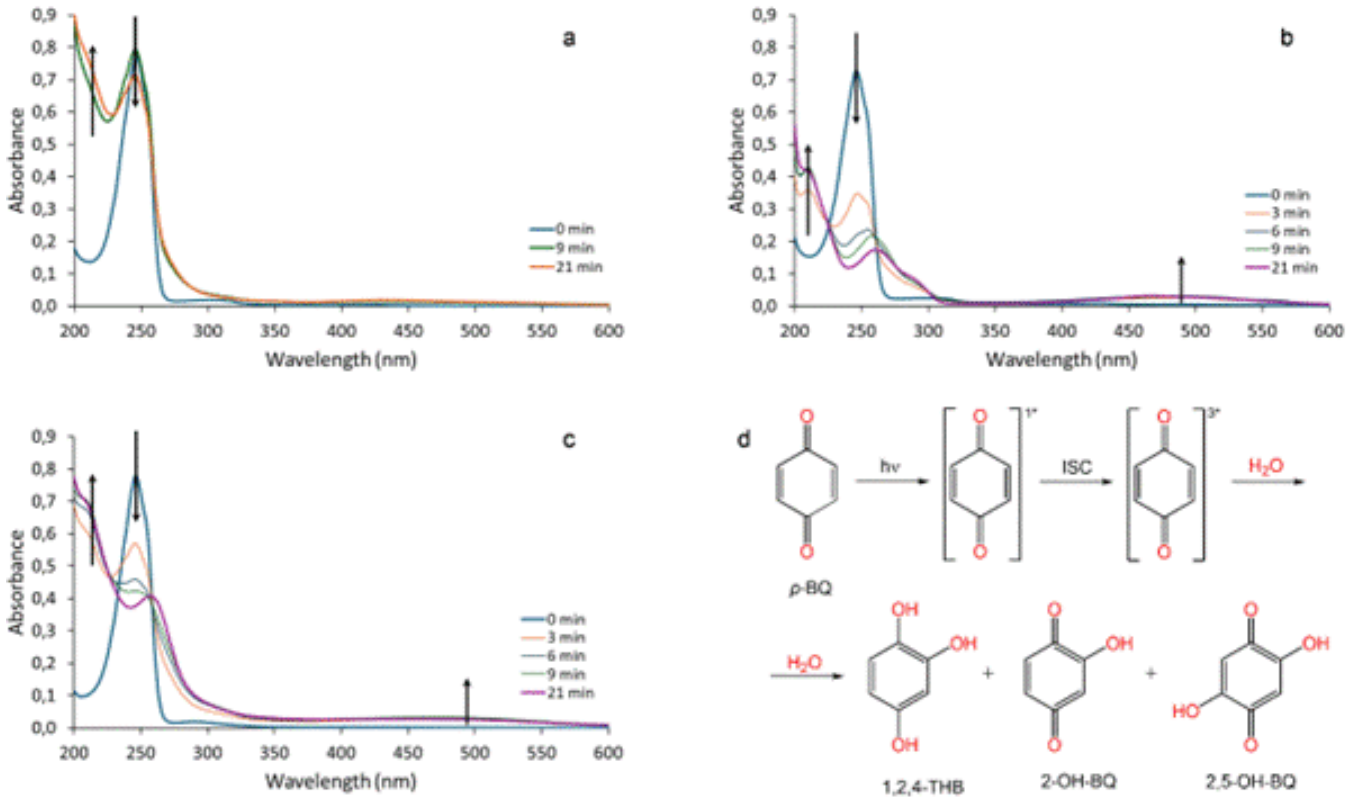

Figure 9 UV-vis spectral changes of 30 µM p-BQ aqueous solution with SnO_2 in dark (a), under 365 nm irradiation without (b) and with SnO_2 (c). Possible photolytic degradation products of p-BQ in protic solvent upon excitation at 365 nm, intersystem crossing from singlet excited state to triplet excited state and direct reaction with water (d).

Moving from water to acetonitrile different results are evident. No significant spectral changes are observable for a 30 µM solution of *p*-BQ in ACN under stirring in dark for 21 minutes with SnO_2 (Figure 10, panel a) or irradiated at 365 nm without SnO_2 (Figure 10, panel b). These outcomes allow us to exclude both physisorption of the molecule onto the metal oxide and any self-quenching mechanism. On the contrary when the *p*-BQ solution is irradiated in presence of SnO_2, a sensible decrease of the corresponding absorption maximum at 243 nm (-55%) is clearly discernible, flanked by a slight increase at about 290 nm (Figure 10, panel c),), suggesting the formation of hydroquinone (H_2Q) or benzosemiquinone (BSQ), that then further degrade in other by-products. These outcomes are in line with the formation of the superoxide anion in non protic solvent catalysed by SnO_2.

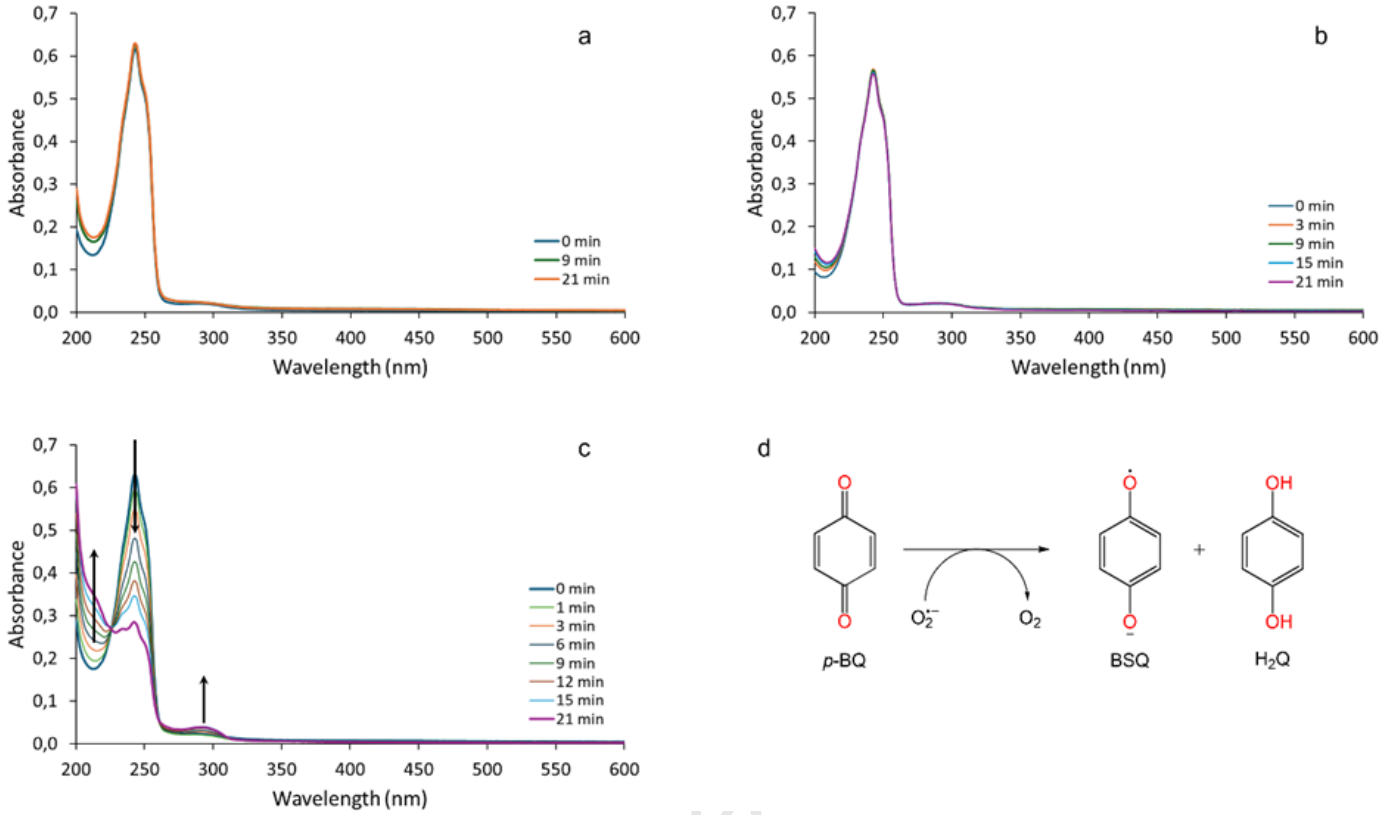

Figure 10 a) UV-vis spectral changes of 30 μM p-BQ ACN solution with SnO_2 in dark (a), under 365 nm irradiation without (b) and with SnO_2 (c). Possible photocatalytic degradation products of p-BQ in aprotic solvent upon excitation at 365 nm, generation of superoxide anion by SnO_2 and subsequent reduction of p-BQ (d).

In light of these results we can reasonably conclude that, once irradiated, SnO_2 nanoparticles have the capability of generating superoxide anions even in water though the extremely low lifetime of this species in this solvent does not allow for any direct attack to *p*-BQ, that in turn undergoes to self-quenching due to fast reaction of its excited triplet state with water molecules, generating hydroxylated byproducts. Nevertheless, in the case of CV dye, since its absorbance remains substantially unchanged upon irradiation in water (see figure 5b) thus excluding a self-quenching mechanism, it is plausible to suppose that the generation of superoxide anion can be a first step of the photocatalytic process, leading to much more reactive species, such as hydroxyl radicals (• OH), that in turn can attack the CV methine carbon atom starting the degradation pathway of the dye.

A similar mechanism can be envisaged for SnO as well, though the smaller energy bandgap of the material (2.7 *vs* 3.6 eV), likely induces the photocatalytic oxidation at a much lower extent, in compliance with the reduced performances under -irradiation.

5. Conclusions

In this work, the syntheses of tin monoxide (SnO) and tin dioxide (SnO_2) in choline chloride:urea 1:2 Deep Eutectic Solvent are reported. The latter system was obtained through a facile, innovative, and here reported for the first time, modification of the legacy DES-synthesis method available in the literature, which yields SnO. The novel procedure comprises the simple addition of the powerful but substantially atoxic and unharmful sodium percarbonate, the main component of household “oxygen bleaches”, at molar ratios at least 3:1 with respect to tin chloride. Both syntheses described lead to pure tin mono- or dioxide in nanoparticular form, as was ascertained by several investigations, that prove that in both cases the materials are nano-sized and possess a large surface extent. The latter features, paired to

the large electronic band-gap of the materials, particularly in SnO_2 case, confer to both systems one of the most coveted property metal oxides can have, namely the capability of acting as catalyst in chemical reactions. Indeed, the synthesized systems have proved to be very efficient in the degradation of crystal violet (CV), a dye known for its negative impact on the environment. The performances in dye removal (discolouration) from its solutions containing SnO or SnO_2 or no catalyst were evaluated under various operating conditions, i. e. dark and irradiation with ambient light, visible light and UV light, in order to identify the most effective and reliable methodology. The results obtained point out that both oxides are capable of discolouring the solution, even in the dark, but the maximal effect is observed when light, in particular UV radiation, is shone on to the solution, suggesting a cooperative synergy of physical absorption and photo-induced chemical processes. UV light allowed for significantly greater removal than other conditions, highlighting the role of photocatalysis in this bleaching process, and SnO_2 demonstrated greater efficiency than SnO under all experimental conditions, thanks to both a greater adsorption capacity on its surface and a higher photocatalytic activity. The best result was achieved using SnO_2 and UV light, that were capable of removing CV from the solution, as signalled by UV-Vis absorption quenching, by a large figure such as 96%, in only 21 minutes. Prompted by this very successful results, new DESs and additives are being investigated, together with further disentanglement between absorption and photocatalysis sub-processes through physical adsorption experiments (e. g. BET surface area analysis), the optimization of catalyst recyclability and the full appraisal and quantification of the degradation products, so that a real claim about the outperforming features of this new class of materials can be issued, and extensive application of the methodology in water remediation strategies can be made.

Author contributions

Lorenzo Gontrani: Writing–original draft, Writing–review & editing, Conceptualization, Investigation. Francesca A. Cotirlan: Investigation, Visualization, Angelo Lembo: Investigation, Validation, Resources, Writing–review & editing. Elvira M. Bauer: Investigation, Data curation, Marilena Carbone: Writing – review & editing, Validation, Supervision, Project administration.

Conflicts of interest

There are no conflicts to declare.

Data availability

The data supporting this article have been included as part of the Supplementary Information. Crystallographic data are available from the databases cited in the references.

Acknowledgements

L.G, M.C. and E.M.B. acknowledge GREEN3 (CUP E53D23005230006; project number: 2022F4YZP9) project funded by the Ministero dell'Università e della Ricerca within the PRIN 2022 program

References

[1] B. Lellis, C.Z. Fávaro-Polonio, J.A. Pamphile, J.C. Polonio, Biotechnol. Res. Innov. 3 (2019) 275–290.

[2] S. Mani, R.N. Bharagava, in: 2016, pp. 71–104.

[3] M.S. Sultana, M.S. Islam, R. Saha, M. Al-Mansur, Bangladesh J. Sci.Ind. Res. 44 (1970) 65–80.

[4] M. Saji, S. Taguchi, K. Uchiyama, E. Osono, N. Hayama, H. Ohkuni, J. Hosp. Infect. 31 (1995) 225–228.

[5] F. Le Curieux, J.M. Gohlke, A. Pronk, W.C. Andersen, G. Chen, J.-L. Fang, K. Mitrowska, P.J. Sanders, M. Sun, G.A. Umbuzeiro, T. Umemura, L. Benbrahim-Tallaa, F. El Ghissassi, Y. Grosse, W. Gwinn, D. Middleton, E.

Suonio, F. Chung, A. Miranda-Filho, H. Mattock, K.Z. Guyton, M.K. Schubauer-Berigan, Lancet Oncol. 22 (2021) 585–586.

[6] N. Littlefield, Fundam. Appl. Toxicol. 5 (1985) 902–912.

[7] M. Douvoyiannis, C. Swank, Pediatr. Emerg. Care 32 (2016) 614–615.

[8] W.T. Parker, P.S. Binder, Am. J. Ophthalmol. 87 (1979) 340–343.

[9] S.P. Dhir, S.K. Sharma, V.P. Munjal, A. Gupa, Indian J. Ophthalmol. 30 (1982).

[10] S. Mani, R.N. Bharagava, in: 2016, pp. 71–104.

[11] Md.K. Hasan, A. Shahriar, K.U. Jim, Heliyon 5 (2019) e02145.

[12] M.S. Sultana, M.S. Islam, R. Saha, M. Al-Mansur, Bangladesh J. Sci.Ind. Res. 44 (1970) 65–80.

[13] S.J. Kwak, J. Park, Y. Sim, H. Choi, J. Cho, Y.-M. Lee, PeerJ 12 (2024) e17442.

[14] P. Durango-Usuga, F. Guzmán-Duque, R. Mosteo, M. V. Vazquez, G. Peñuela, R.A. Torres-Palma, J. Hazard. Mater. 179 (2010) 120–126.

[15] H.-J. Fan, S.-T. Huang, W.-H. Chung, J.-L. Jan, W.-Y. Lin, C.-C. Chen, J. Hazard. Mater. 171 (2009) 1032–1044.

[16] S. Gautam, H. Agrawal, M. Thakur, A. Akbari, H. Sharda, R. Kaur, M. Amini, J. Environ. Chem. Eng. 8 (2020) 103726.

[17] A. Aeisyah, M.H.S. Ismail, K. Lias, S. Izhar, Res. J. Chem. Environ.. 18 (2014) 91–102.

[18] U.M. Ismail, S.A. Onaizi, M.S. Vohra, Environ. Technol. Innov. 33 (2024) 103456.

[19] A.J. Leong, N. Nyuk-Ting, N.S.Mohd. Nor, U. Baig, W.A.W. Ibrahim, Mohd.M. Sanagi, A.S.A. Keyon, in: 2019, p. 020013.

[20] J. Mittal, R. Ahmad, M.O. Ejaz, A. Mariyam, A. Mittal, Int. J. Phytoremediation 24 (2022) 796–807.

[21] D. Nunes, A. Pimentel, A. Gonçalves, S. Pereira, R. Branquinho, P. Barquinha, E. Fortunato, R. Martins, Semicond. Sci. Technol. 34 (2019) 043001.

[22] M. Fernández-García, J.A. Rodriguez, in: Encyclopedia of Inorganic and Bioinorganic Chemistry, Wiley, 2011.

[23] U.P.M. Ashik, A. Viswan, S. Kudo, J. Hayashi, in: Applications of Nanomaterials, Elsevier, 2018, pp. 45–82.

[24] J. Wang, N. Umezawa, H. Hosono, Adv. Energy Mater. 6 (2016).

[25] M.S. Moreno, R.C. Mercader, A.G. Bibiloni, J. Phys. Cond. Matt. 4 (1992) 351–355.

[26] M.A. Mäki-Jaskari, T.T. Rantala, Model. Simul. Mat. Sci. Eng. 12 (2004) 33–41.

[27] F. Lawson, Nature 215 (1967) 955–956.

[28] C.G.M. Decroly, R. Acad. Sci., Paris 261 (1965) 2659.

[29] M.S. Moreno, A. Varela, L.C. Otero-Díaz, Phys.Rev. B 56 (1997) 5186–5192.

[30] R.M. Organ, J.A. Mandarino, Can. Mineral 10 (1971) 916.

[31] W.H. Baur, Acta Crystallogr. 9 (1956) 515–520.

[32] M. Batzill, U. Diebold, Prog. Surf. Sci. 79 (2005) 47–154.

[33] J. Pannetier, G. Denes, Acta Crystallogr B 36 (1980) 2763–2765.

[34] A. Walsh, G.W. Watson, Phys. Rev. B 70 (2004) 235114.

[35] J. Savioli, A.L. Gavin, A.K. Lucid, G.W. Watson, in: Tin Oxide Materials, Elsevier, 2020, pp. 11–39.

[36] Md.A. Islam, J.R. Mou, Md.F. Hossain, A.M.M.T. Karim, Md. Kamruzzaman, Md.S. Hossain, J. Solgel Sci. Technol. 96 (2020) 304–313.

[37] S. Umnov, O. Asainov, V. Temenkov, IOP Conf. Ser. Mater. Sci. Eng. 124 (2016) 012148.

[38] B. Borah, S. Banerjee, B.K. Allam, Tetrahedron Green Chem 4 (2024) 100048.

[39] C. Liu, W. Wang, F. Wu, J. Zhang, C. Chen, P. Cheng, Y. Zhu, S. Zhang, G. Seong, Chem. Rec. 25 (2025).

[40] O. Renault, A.V. Tadeev, G. Delabouglise, M. Labeau, Sens. Actuators B: Chem 59 (1999) 260–264.

[41] M. Batzill, Sensors 6 (2006) 1345–1366.

[42] M. Batzill, U. Diebold, Prog. Surf. Sci. 79 (2005) 47–154.

[43] H.H. Kristoffersen, J.Ø. Hansen, U. Martinez, Y.Y. Wei, J. Matthiesen, R. Streber, R. Bechstein, E. Lægsgaard, F. Besenbacher, B. Hammer, S. Wendt, Phys. Rev. Lett. 110 (2013) 146101.

[44] H. Shi, H. Liu, Z. Li, W. Wang, X. Shao, Phys. Chem. Chem. Phys. 22 (2020) 27077–27083.

[45] M. A. M. Akhir, S.A. Rezan, K. Mohamed, M.M. Arafat, A.S.M.A. Haseeb, H.L. Lee, Mater. Today Proc. 17 (2019) 810–819.

[46] S. Zong, Y. Zhang, J. Cao, C. Qin, H. Bala, Y. Wang, Langmuir 40 (2024) 10814–10824.

[47] M. Bonomo, L. Gontrani, A. Capocefalo, A. Sarra, A. Nucara, M. Carbone, P. Postorino, D. Dini, J. Mol. Liq. 319 (2020) 114292.

[48] M.C. Gutiérrez, D. Carriazo, C.O. Ania, J.B. Parra, M.L. Ferrer, F. del Monte, Energy Environ. Sci. 4 (2011) 3535.

[49] M. Busato, V. Di Lisio, A. Del Giudice, P. Tomai, V. Migliorati, L. Galantini, A. Gentili, A. Martinelli, P. D'Angelo, J. Mol. Liq. 331 (2021) 115747.

[50] L. Gontrani, N. V. Plechkova, M. Bonomo, ACS Sustain. Chem. Eng. 7 (2019) 12536–12543.

[51] A.P. Abbott, G. Capper, S. Gray, ChemPhysChem 7 (2006) 803–806.

[52] L. Gontrani, D.T. Donia, E. Maria Bauer, P. Tagliatesta, M. Carbone, Inorg. Chim. Acta 545 (2023) 121268.

[53] L. Gontrani, L. Casoli, O. Russina, E.M. Bauer, M. Carbone, Mater. Adv. 6 (2025) 2154–2159.

[54] L. Gontrani, P. Tagliatesta, D.T. Donia, E.M. Bauer, M. Bonomo, M. Carbone, Molecules 27 (2022) 2045.

[55] S. Sugiarto, U. Aloka Weerasinghe, J. Kinyanjui Muiruri, A. Yu Qing Chai, J. Chee Chuan Yeo, G. Wang, Q. Zhu, X. Jun Loh, Z. Li, D. Kai, Chem. Eng. J, 499 (2024) 156177.

[56] J. Richter, M. Ruck, Molecules 25 (2019) 78.

[57] H. Jia, F. Zhang, J. Sun, F. Chong, Chem. Eng. J, 524 (2025) 169516.

[58] H. Jia, F. Zhang, C. Zhu, J. Sun, X. Xie, Colloids Surf. A Physicochem. Eng. Asp. 679 (2023) 132594.

[59] H. Jia, M. Dong, Z. Yuan, J. Chen, Z. Gong, J. Shao, Ceram. Int. 47 (2021) 23249–23258.

[60] H. Zheng, C.-D. Gu, X.-L. Wang, J.-P. Tu, J. Nanoparticle Res. 16 (2014) 2288.

[61] J. Chen, M.C. Ali, R. Liu, J.C. Munyemana, Z. Li, H. Zhai, H. Qiu, Chin. Chem. Lett.. 31 (2020) 1584–1587.

[62] L. Gontrani, P. Tagliatesta, D.T. Donia, E.M. Bauer, M. Bonomo, M. Carbone, Molecules 27 (2022) 2045.

[63] B.B. Hansen, S. Spittle, B. Chen, D. Poe, Y. Zhang, J.M. Klein, A. Horton, L. Adhikari, T. Zelovich, B.W. Doherty, B. Gurkan, E.J. Maginn, A. Ragauskas, M. Dadmun, T.A. Zawodzinski, G.A. Baker, M.E. Tuckerman, R.F. Savinell, J.R. Sangoro, Chem. Rev. 121 (2021) 1232–1285.

[64] E.L. Smith, A.P. Abbott, K.S. Ryder, Chem. Rev. 114 (2014) 11060–11082.

[65] H. Qin, X. Hu, J. Wang, H. Cheng, L. Chen, Z. Qi, Green Energy Environ. 5 (2020) 8–21.

[66] Y. Liu, J.B. Friesen, J.B. McAlpine, D.C. Lankin, S.-N. Chen, G.F. Pauli, J. Nat. Prod. 81 (2018) 679–690.

[67] S. Nejrotti, A. Antenucci, C. Pontremoli, L. Gontrani, N. Barbero, M. Carbone, M. Bonomo, ACS Omega 7 (2022) 47449–47461.

[68] K.A. Pishro, M.H. Gonzalez, RSC Adv. 14 (2024) 14480–14504.

[69] M.R. Rabiei, M. Hosseini, G. Xu, Microchem J 203 (2024) 110909.

[70] R. Cui, Y. Ran, D. Shu, Q. Huang, Q. Song, H. Wang, J. Zhu, W. Yuan, J. Environ. Manage. 377 (2025) 124670.

[71] G.R. Medders, F. Paesani, J. Chem. Theory Comput. 11 (2015) 1145–1154.

[72] J. Köhler, J. Tong, R. Dinnebier, A. Simon, Z. Anorg. Allg. Chem. 638 (2012) 1970–1975.

[73] V. Mackert, T. Winter, S. Jackson, R. Kalia, A. Levish, S. Lukic, J. Geiss, M. Winterer, J. Phys. Chem. C 127 (2023) 17389–17405.

[74] S. Denman, S. Jameel, J. Hay, J.K. Sugden, Dyes Pigm 30 (1996) 67–72.

[75] N. Khera, J. Pethaiyan, Nanoscale Adv. (2025).

[76] S. Shabna, J.E. Shaji, S.S.J. Dhas, S. Suresh, A. Aravind, S.A. Thomas, V.S. Vinita, J. Samuel, C.S. Biju, J. Clust. Sci. 35 (2024) 597–606.

[77] I. Hussain, A. Bibi, M.I.K. Khail, T. Zhenbo, R. Khan, Z. Hussain, F.-G. Yu, C.Z. Zao, M.K. Khan, J. Water Process Eng. 77 (2025) 108511.

[78] O. Fónagy, E. Szabó-Bárdos, O. Horváth, J. Photochem. Photobiol. A Chem. 407 (2021) 113057.

[79] J.T. Schneider, D.S. Firak, R.R. Ribeiro, P. Peralta-Zamora, Phys. Chem. Chem. Phys. 22 (2020) 15723–15733.

[80] Y. Wang, J. Li, Z. Zhou, R. Zhou, Q. Sun, P. Wu, Nat. Commun. 12 (2021) 526.

[81] Y. Wang, H. Chen, C. Li, P. Wu, Dyes and Pigments 170 (2019) 107635.

[82] K. Tanaka, T. Miura, N. Umezawa, Y. Urano, K. Kikuchi, T. Higuchi, T. Nagano, J. Am. Chem. Soc. 123 (2001) 2530–2536.

[83] A.B. Ormond, H.S. Freeman, Dyes and Pigments 96 (2013) 440–448.

[84] M. Ethirajan, Y. Chen, P. Joshi, R.K. Pandey, Chem. Soc. Rev. 40 (2011) 340–362.

[85] J. Tian, B. Huang, M.H. Nawaz, W. Zhang, Coord. Chem. Rev. 420 (2020) 213410.

[86] D. Wang, L. Zhao, H. Ma, H. Zhang, L.-H. Guo, Environ. Sci. Technol. 51 (2017) 10137–10145.

[87] A. Guerreiro, N. Chatterton, E.M. Crabb, J.P. Golding, Cancer Nanotechnol. 10 (2019) 10.

[88] A. Khaledian, S. Zakavi, Inorg. Chem. Commun. 167 (2024) 112727.

[89] A. Lembo, M. Demingo, L. Gontrani, C. Ricci, A. Leoni, M. Carbone, P. Tagliatesta, Inorg. Chem. 64 (2025) 24450–24468.

[90] P. Pushpanandan, Y.K. Maurya, T. Omagari, R. Hirosawa, M. Ishida, S. Mori, Y. Yasutake, S. Fukatsu, J. Mack, T. Nyokong, H. Furuta, Inorg. Chem. 56 (2017) 12572–12580.

[91] P.E. Kesavan, V. Pandey, M. Ishida, H. Furuta, S. Mori, I. Gupta, Chem. Asian J. 15 (2020) 2015–2028.

[92] X. Ding, K. Zhao, L. Zhang, Environ. Sci. Technol. 48 (2014) 5823–5831.

[93] M. Hayyan, M.A. Hashim, I.M. AlNashef, Chem. Rev. 116 (2016) 3029–3085.

[94] O. Fónagy, E. Szabó-Bárdos, O. Horváth, J. Photochem. Photobiol. A Chem. 407 (2021) 113057.

[95] K.C. Kurien, P.A. Robins, J. Chem. Soc. B (1970) 855–859.

[96] J. von Sonntag, E. Mvula, K. Hildenbrand, C. von Sonntag, Chem-Eur. J, 10 (2004) 440–451

Declaration of interests

☒ The authors declare that they have no known competing financial interests or personal relationships that could have appeared to influence the work reported in this paper.

☐ The authors declare the following financial interests/personal relationships which may be considered as potential competing interests:

Lorenzo Gontrani graduated in chemistry (summa cum laude) at Rome Sapienza university in 1998 and received a PhD degree in Chemical Sciences at Pisa University in 2002. At present, he is associate professor of Inorganic Chemistry in the University of Rome Tor Vergata. He has a solid background in the computational description of complex chemical systems (ab initio, classical molecular dynamics), fully integrated with experimental techniques, like spectroscopic and diffrattometric analyses. In particular, his current research interests are mainly focused on

- Synthesis of metal oxide nanoparticles with traditional and innovative media, like Deep Eutectic Solvents and ionic liquids
- Powder XRD analysis (Rietveld method), SEM microscopy and DRS measurements of nanoparticles and pigments
- Calculation of electronic properties (bandgap and UV-Vis spectra) of dyes for DSSC, in various environments

He took part to various national and international research projects as principal investigator or as investigator.

He co-authored 117 peer-reviewed papers, 2 book chapters, has edited one monograph dedicated to the structural aspects of ionic liquids and serves as reviewer of several journals in the field of computational chemistry, ionic liquids/DES and materials science. He is member of Società Chimica Italiana and of some editorial committees. He reported the results of his research in several national and international congresses, also as invited speaker.

Graphical abstract

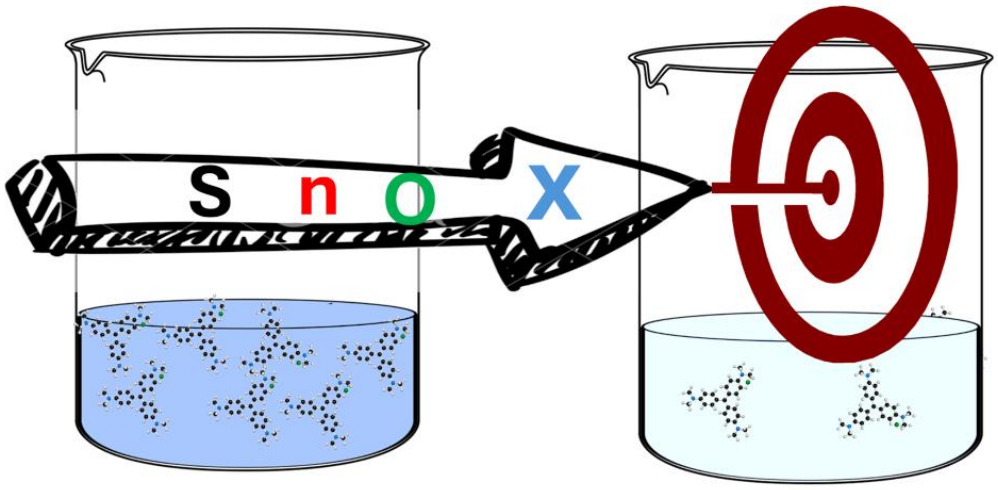

Highlights

- SPC addition to eco-friendly DES media leads to SnO_2 NPs with large specific surface
- SPC creates a highly oxidizing environment within DES, preventing its air shielding
- SnO_2 scores an impressive 96% dye reduction under UV light in only 21 minutes
- The fast and low-waste synthesis can be performed also in low-resource settings
- Good dye-removal activity is recognized in both SnO and SnO_2 nanoparticles